

BRDF Analysis of Different Land Cover Types Using Aerial and Satellite Imagery

ALEXANDER KÖHN¹

Abstract: Bi-directional reflectance distribution function (BRDF) effects are an important factor influencing the reflectance of the land surface, especially at large off-nadir angles. This work demonstrates the information gain from using multi-angular images from a low-cost aerial camera system as well as means to radiometrically calibrate these images facing unknown camera parameters. Land surface BRDF are estimated by inverting four semi-empirical kernel-driven models. A novel model is proposed utilising the same data sources as the other methods but featuring a more explicit geometrical modelling approach using the OpenGL library. Although some issues with the current model remain, an improved version may be a useful addition to conventional methods.

1 Introduction

Surface anisotropy describes the property of virtually all natural surfaces to reflect light differently strong in different directions. While spectral reflection variance is often due to chemical composition of the target surface, angular variance tends to primarily depend on textural properties (BARNSELY et al. 2004). In a simplified sense, rough surfaces will result in a more Lambertian scattering behaviour while very smooth surfaces (e.g. polished metal, water) have a strong directional component which is hereafter referred to as hotspot. Surface anisotropy is formalised as the bi-directional reflectance distribution function (BRDF) where the reflectance f_r for a given reflection angle (φ_r, θ_r) and an illumination angle (φ_i, θ_i) at wavelength λ is expressed by

$$f_r(\varphi_i, \varphi_r, \theta_i, \theta_r, \lambda) = \frac{dL_r(\varphi_i, \varphi_r, \theta_i, \theta_r, \lambda)}{dE_i(\varphi_i, \theta_i, \lambda)} = \frac{dL_r(\varphi_i, \varphi_r, \theta_i, \theta_r, \lambda)}{L_i(\varphi_i, \theta_i, \lambda) \cos \theta_i d\omega} [sr^{-1}],$$

i.e. the ratio of reflected radiance dL_r to irradiance dE_i of an infinitesimal area dA (NICODEMUS et al. 1977). BRDF is an important factor that needs to be corrected when working with wide-angle sensors such as AVHRR, MODIS and MERIS where anisotropic effects become especially pronounced in the off-nadir field-of-view (WANNER et al. 1995). Nonetheless, the additional information content from multi-angular imagery can be applied to classify land surfaces that are poorly distinguishable in the spectral domain (BARNSELY et al. 1997). BRDF is still widely ignored in land surface studies on a local scale, certainly in parts due to the prevalence of sensors featuring a narrow field of view with little or no tilting capabilities such as LANDSAT or Sentinel where BRDF effects are not particularly apparent (KOUKAL & SCHNEIDER 2010). More recently, commercial high-resolution platforms with considerable tilting capabilities emerged to be more responsive to customer needs (e.g. Ikonos, WorldView, Pléiades and SkySat). This

¹ Saarland University, Department of Computer Science, Campus, D-66123 Saarbrücken, E-Mail: s8alkoeh@stud.uni-saarland.de

trend demands a renewed level of awareness for angular effects but also provides new opportunities to investigate land surface BRDF.

The equation above implies that an infinite number of observations over the whole viewing hemisphere is required to accurately describe the BRDF of a given land surface. In reality, especially when using airborne or spaceborne sensors for measuring BRDF, interpolating over the data points is impractical due to the sparseness of observations and the tendency to angular bias of satellite orbits and flight paths (KOUKAL & ATZBERGER 2012). For that reason, special models have been developed to incorporate some assumptions on the target surface to more accurately predict the BRDF when facing sparse angular sampling. Hence, physical models generally achieve the most accurate descriptions of radiative transfer but are rather impractical for model inversion (CHEN et al. 2000; KOUKAL & ATZBERGER 2012). On the other hand, kernel-driven models attempt to describe reflectance as a linear combination of kernels, that are functions that simulate a specific scattering behaviour that contributes to the final BRDF. Inverting these models is relatively straightforward since they can be considered as an overdetermined system of linear equations which can be solved by minimising a linear least squares problem (LEWIS 1995; WANNER et al. 1995).

Hence, BRDF studies may benefit from a similar viewing geometry as common for photogrammetric purposes. Interestingly, there is little research on how such camera systems can be applied to sample BRDF which in turn may be used to normalise images on a physical basis. Moreover, height information from photogrammetrically derived digital surface models (DSM) can be used to explicitly formulate kernel functions for geometrical shadowing and diffuse shading which could improve BRDF model accuracy compared to conventional models while relying on the same input data.

2 Methodology

In this study, data from the aerial DLR 3K camera system and the Pléiades constellation are examined. The airborne sensor is used to answer the question whether a low-cost camera system can be used for BRDF studies. The goal here is to radiometrically correct the images and, by reproducing the methodology of BARNSELY et al. (1997), to generate multi-angular composite images displaying the information content. The second part features a comparison between four BRDF models including a novel one using high-resolution Pléiades data.

2.1 Datasets

The first dataset consists of aerial imagery acquired by the DLR 3K imaging system during a flight campaign on September 17th 2015 over the Kranzberger Forst near Freising, Germany. With one nadir-looking and two laterally mounted oblique-looking off-the-shelf DSLR cameras, it has a field-of-view of 110° in across-track direction and 31° in along-track direction (KURZ et al. 2012). The solar azimuth angles were almost perpendicular to the flight paths which rendered the oblique-looking images especially valuable for BRDF studies. This is due to the tendency of the solar plane to contain most information about surface anisotropy (KIMES 1983). However, since the respective flight paths over the area of interest were several tens of minutes apart, only

successive images from a single camera were used to prevent changes in the solar position to obscure the results.

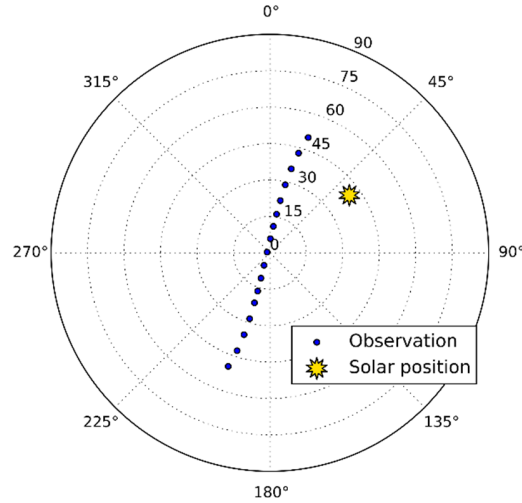


Fig. 1: Polar plot of the Pléiades viewing and illumination geometry

The second dataset comprises a set of 18 Pléiades images acquired over Melbourne, Australia on February 25th 2012 during a single overpass using the persistent surveillance imaging mode. This implies a good angular coverage approximately along the solar plane between zenith angles of -50.03° and $+49.8^\circ$ (Fig. 1). For all practical purposes, the solar incidence angle can be considered constant due to an overall time interval of 03:30 min between the first and the last image. Two small subsets with relatively homogeneous land cover were manually selected, one representing a suburban residential area while the other one was taken from a salt marsh.

2.2 Radiometric and geometric calibration

3K imagery is not designed for radiometric studies and is, by default, recorded in the JPEG format which implies a compression from 16-bit RAW to 8-bit grey values and, more important, that both camera response curve and white balance factor are not preserved which are needed for radiometric calibration. The whole conversion procedure can be expressed by

$$L = \frac{g(B)}{w_i e M}, \text{ with } e = \frac{\pi s t}{k^2},$$

where L is the scene radiance, g the inverted camera response curve, B the raw digital number, w_i the white-balance factor for band i , e the effective exposure, M the vignetting coefficient, s the sensor sensitivity (ISO), t the shutter speed and k the aperture value (D'ANGELO 2007).

The camera response curve was estimated by plotting grey values of simultaneously taken RAW and JPEG photos against each other and taking the most abundant RAW value for each 8-bit JPEG value which was then saved to a look-up table (Fig. 2, right). Since weight balance appears to be least pronounced in the green band (D'ANGELO 2007), only this band was transformed. Finally, the vignetting coefficient of the camera lens was determined by finding the weights to a radial polynomial (D'ANGELO 2007) using the physically-based photo stitching software hugin on panorama photos of one of the 3K cameras. This resulted in individual vignetting curves for all f-numbers between 3.2 and 9.9 (Fig. 2, left).

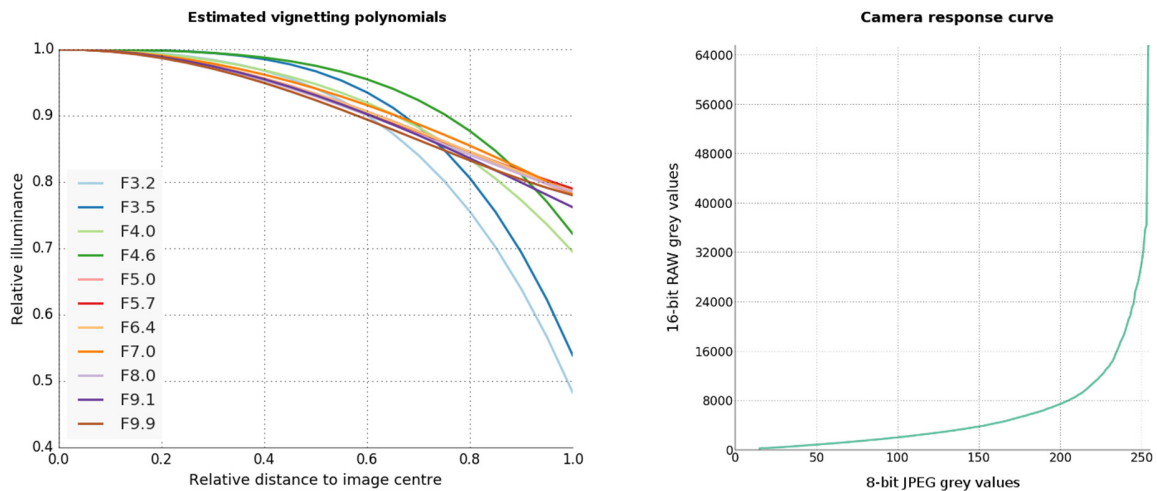


Fig. 2: Radiometric calibration results: estimated vignetting curves (left) and camera response curve (right)

Like BARNSELY et al. (1997), 3K imagery was not atmospherically corrected in these experiments which, however, will be necessary in future studies if those data are used for BRDF modelling. Geometric calibration was performed using highly accurate rational polynomial coefficients (RPC) and a 90 m SRTM DEM. Note that perfect orthorectification is not desired here since perspectival deformations are important contributors to the BRDF of a land surface. This will, on the other hand, compromise the visualisation of the anisotropy of obstructions, i.e. canopies and roof tops. The Pléiades data used ATCOR 2 as atmospheric correction procedure (RICHTER & SCHLÄPFER 2005) since this method assumes a planar surface which is critical for later modelling. Unfortunately, the Pléiades DIMAP V2 format has a default band combination Red-Green-Blue-NIR which led to a mix-up in the correction procedure and ultimately implies that the modelling results have no real meaning (R. RICHTER, personal communication, 2016). Nonetheless, this does not compromise the validity of the assessment of different BRDF models since all images are still comparable in relative terms. The atmospherically corrected images were then projected onto a 90 m SRTM DEM in case of the three conventional methods. However, the design of the fourth model required an orthorectified input which is why a photogrammetric DSM was used instead.

2.3 BRDF model descriptions

All of the implemented models are kernel-driven. The first one is the Walthall model which is a simple empirical description of the BRDF of canopies and one of the first kernel-driven models (WANNER et al. 1995). By contrast, the semi-empirical Roujean model formulates a volumetric scattering kernel, dubbed RossThick, a geometric kernel to simulate macroscopic shadowing and an isotropic kernel for Lambertian reflectance (WANNER et al. 1995). The third tested model is the RossThick-LiSparse (RTLs) model which adapts the general design of the Roujean model but exchanges the geometric Roujean kernel by the LiSparse kernel which in turn is based on the Li-Strahler model of mutual shadowing (WANNER et al. 1995). Both geometric kernels are analytical descriptions of the shadowing effects of randomly scattered primitives on a horizontal plane.

Since BRDF partly depends on the macroscopic geometry of the scene, utilising height information allows to explicitly model shadows and diffuse shading instead of relying on abstract geometrical models as used in the Roujean and RTLS models. The proposed modification of the RTLS model therefore utilises simple Lambertian flat shading and a fast shadow computation technique called shadow mapping while adopting the volumetric RossThick kernel. The rendering has been implemented using OpenGL 4.5.

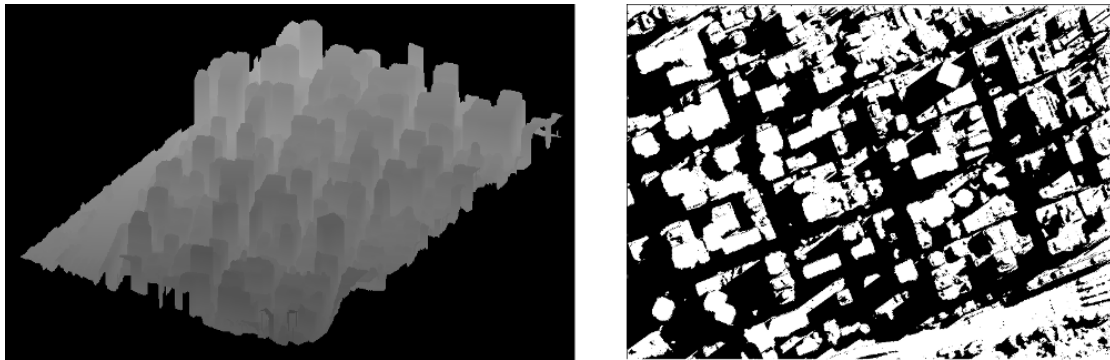


Fig. 3: The principle of shadow mapping: depth map (left) and resulting binary shadow map in nadir view (right).

Shadow mapping (WILLIAMS 1978) is an algorithm where for each pixel a depth value with respect to the light source is computed and saved to a so-called depth map (Fig. 3, left). When transforming the vertices of the geometry from world to light source coordinates, the depth map is queried to decide whether a pixel is visible from the light source. A negative result of this test implies that the pixel must be shadowed. This results in a binary map of hard shadows (Fig. 3, right). Even though, minor modifications would allow to render soft shadows as well, this is unnecessary as the model requires only an averaged value over the larger area of interest.

The original isotropic kernel as used in the Roujean and RTLS model assumes a horizontal plane that diffusely reflects incident light. Since it is invariant of the viewing direction, the kernel function is usually set to unity. This, however, changes if a DSM is used to compute the diffuse reflection for a given illumination angle. An important design decision whose implications will be discussed later was to omit occluded areas for a given viewing direction on the orthorectified image which was also realised by shadow mapping. Since shadows are areas not visible from the position of the sun, one can equally simulate occluded areas by the same algorithm by treating the simulated position of the sensor as light source.

A per-pixel BRDF computation is not feasible at this resolution since this would require a perfect image registration and an even better resolved DSM. Instead, reflectance values over a larger area were averaged which also forgives unrealistic model assumptions in flat shading and hard shadows due to shadow mapping.

2.4 Statistical model assessment

Thorough BRDF model assessment requires substantial effort as simultaneous ground measurements at the time the sensor captures the scene would have to be taken (LUCHT et al. 2000). This, of course, exceeds the capacities of most studies which is why less involving statistical methods are chosen. However, splitting the data into a training, test and verification set

is equally unfavourable due to the sparseness of the data one usually deals with. This makes a representative model assessment rather difficult. Nonetheless, one can assess the goodness of the fit using the coefficient of determination (R^2) or the symmetric mean absolute percentage error (sMAPE). To generate comparable results to KOUKAL & SCHNEIDER (2010), a similar assessment methodology was chosen by computing the sMAPE. A good fit, however, does not necessarily indicate good model performance but could rather imply overfitting to the data, so these results should be handled with care.

3 Results and Discussion

An exemplary result of the angular composites is shown in Fig. 4. The cropland is hardly distinguishable in each of the three images on the left which are selected from five successive images. The angular composite clearly distinguishes between the two crop types and emphasises irregularities. By contrast, forest canopies (upper left corner) and more mature crops exhibit a rather noise-like pattern in the composite due to perspectival deformations.

The angular composites show that the radiometric calibration appears to be very successful in recovering reflectance values and that simple aerial images can be used in radiometric studies. Other results have emphasised crop stains which could prove useful in applications like precision farming, damage assessment or aerial archaeology.

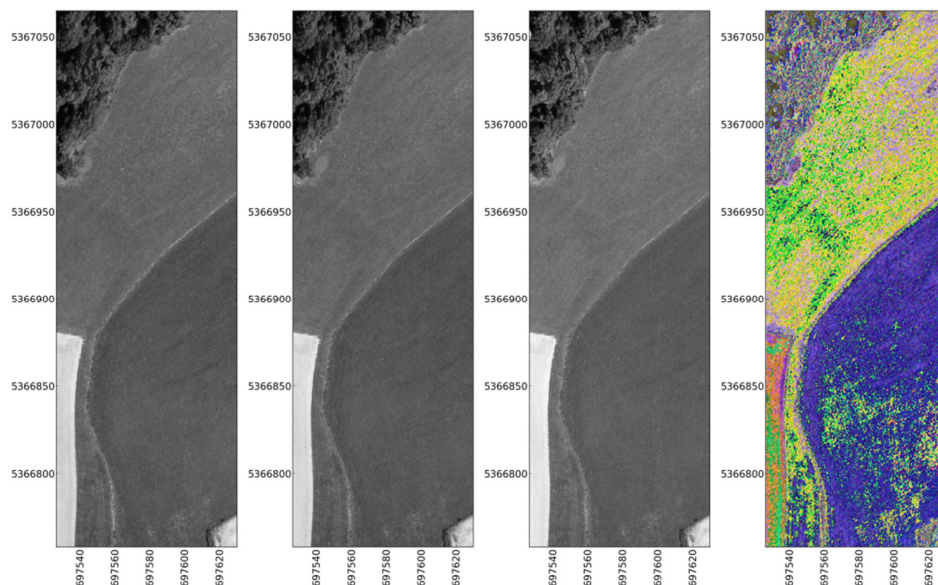


Fig. 4: Three left-looking 3K images (1-3) and the resulting composite image (far right)

A selected BRDF model result of averaged grey values over a residential area is shown in Fig. 5. The three conventional methods performed rather similarly in all selected areas of interest with the RTLS model featuring the most pronounced hotspot which is an observation consistent with KOUKAL & SCHNEIDER (2010). On the other hand, the proposed model produced several severe discrepancies when compared to the other models (Fig. 5, upper row) while agreeing in other cases (Fig. 5, lower row).

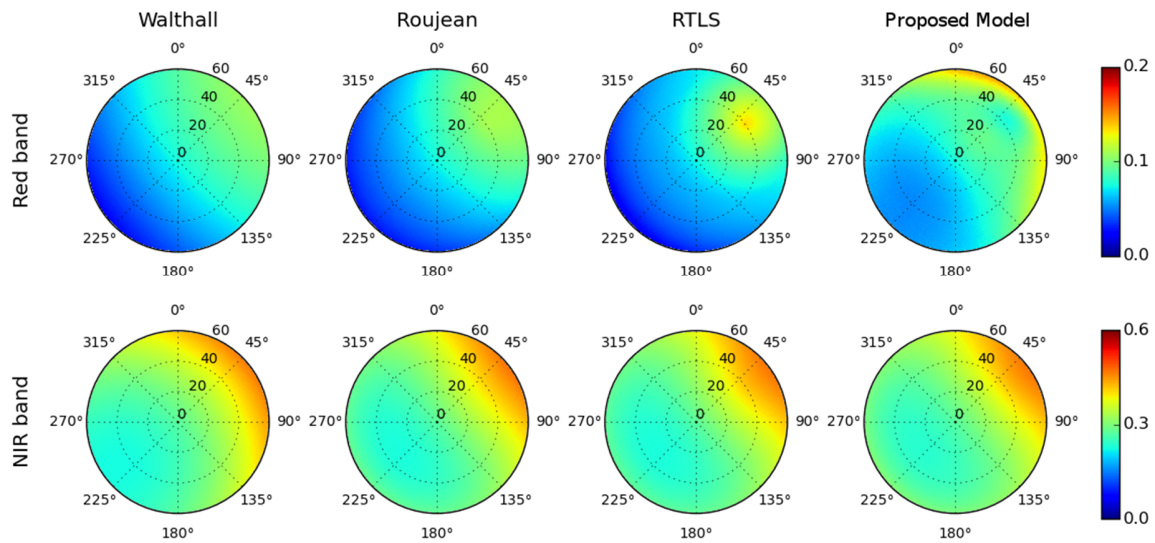


Fig. 5: Simulated BRDF for a suburban residential area in Melbourne, Australia.

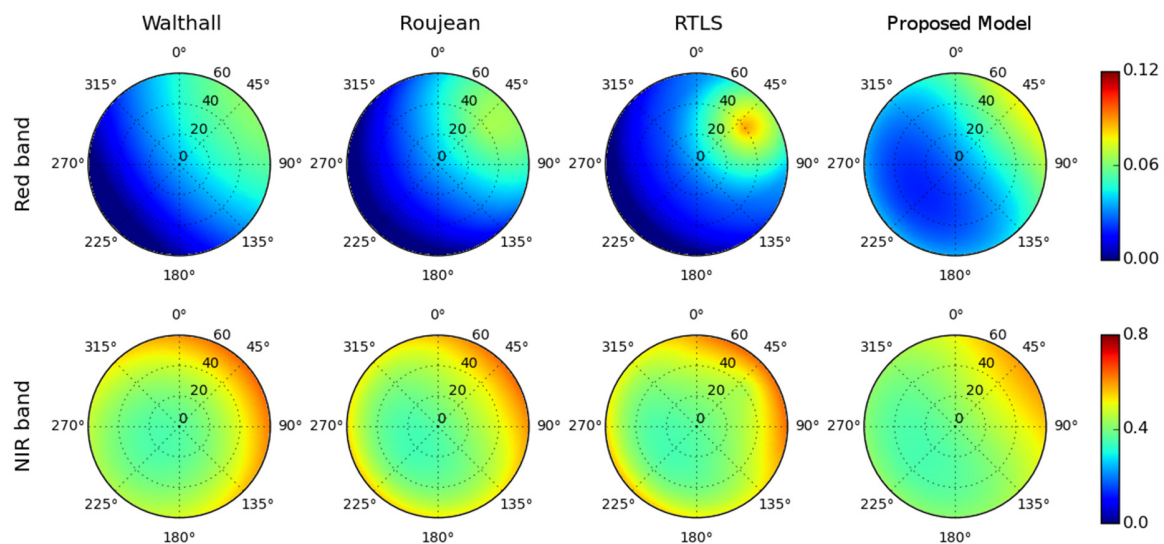


Fig. 6: Simulated BRDF for a salt marsh in Melbourne, Australia.

The results of the salt marsh subset (Fig. 6) highlight the same observations; while the simulated NIR band in the proposed model roughly agrees with the other models, the red band fails to simulate a pronounced hot spot and closer resembles the Walthall model than RTLS. The parameter weights are given in Tab. 1 and 2, respectively. In Tab. 1, the proposed model features a proportionally larger dependence on the geometric and isotropic kernels with respect to the other models.

sMAPE results are visualised in Fig. 7. The statistical results agree with the qualitative assessment with RTLS achieving the smallest error while the proposed model produced the overall highest error over all tested datasets. This was especially apparent in the salt marsh scene (Fig. 7, right).

The disagreement is probably due to masking out occluded areas in the orthorectified image which causes a model bias towards elevated areas at increasing viewing zenith angles. Since vegetation reflects less than the underlying soil in the visible domain (KIMES 1983), the bias towards canopy reflectance is most pronounced in off-nadir directions. Conversely, vegetation is much brighter in the near-infrared domain than its background (KIMES 1983) which also explains the opposite trend found in the respective simulated band.

Tab. 1: Simulated BRDF model weights for the residential area.

Band	Walthall			Roujean		
	k_1	k_2	k_3	k_{iso}	k_{vol}	k_{geo}
Blue	-0.008623	0.039471	0.075886	0.136766	0.059169	0.046739
Green	0.016004	0.057929	0.118468	0.188311	0.169166	0.031151
Red	0.025829	0.058531	0.134191	0.201849	0.199392	0.018721
NIR	0.066232	0.114765	0.275328	0.400207	0.435017	0.016606
Band	RTLS			Proposed Model		
	k_{iso}	k_{vol}	k_{geo}	k_{iso}	k_{vol}	k_{geo}
Blue	0.154369	0.002417	0.043449	-3.385180	0.200868	4.746887
Green	0.201605	0.127868	0.030144	-1.249163	0.224814	1.892070
Red	0.211819	0.170172	0.019618	-0.023008	0.201927	0.237596
NIR	0.409712	0.407628	0.017904	1.059879	0.385021	-1.025671

Tab. 2: Simulated BRDF model weights for the salt marsh.

Band	Walthall			Roujean		
	k_1	k_2	k_3	k_{iso}	k_{vol}	k_{geo}
Blue	-0.009328	0.035356	0.036076	0.082385	0.045860	0.044575
Green	0.030135	0.050245	0.088621	0.133115	0.190759	0.006552
Red	0.042327	0.054977	0.117857	0.165518	0.237521	-0.005591
NIR	0.164078	0.091132	0.365564	0.427633	0.663488	-0.130618
Band	RTLS			Proposed Model		
	k_{iso}	k_{vol}	k_{geo}	k_{iso}	k_{vol}	k_{geo}
Blue	0.095982	-0.001173	0.039016	0.021817	0.112419	0.015625
Green	0.134719	0.184725	0.005435	0.073197	0.197799	0.031250
Red	0.163918	0.243186	-0.004814	0.057714	0.225182	0.093750
NIR	0.387774	0.801343	-0.114339	0.220637	0.459911	0.250000

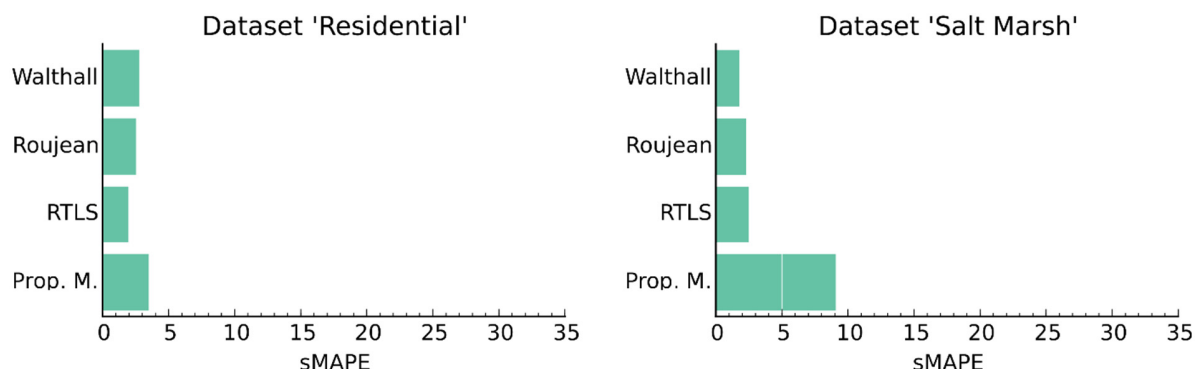


Fig. 7: sMAPE assessment results for both subsets.

These erroneous results might be prevented by using perspectival projections onto a plane instead of occlusion masks which would provide a more realistic simulation of geometric shadowing.

4 Conclusions

In this work, BRDF effects were analysed both qualitatively and quantitatively. First, aerial 3K images meant for photogrammetric purposes were radiometrically calibrated in order to create multi-angular composite images which allowed to assess the surface anisotropy of the given scene. It was possible to visualise the multi-angular information content that can enhance classification approaches solely based on spectral bands. In the second part, four different semi-empirical BRDF models were applied to 18 multi-angular Pléiades images. Among those models, a novel one is proposed based on photogrammetrically derived DSM and computer graphics rendering techniques. The model assessment generally confirms the observations by KOUKAL & SCHNEIDER (2010). Unfortunately, a design flaw in the proposed model caused a bias towards higher elevated areas which is why this model yielded the worst test results.

Future work will clearly focus on fixing these issues and develop the model further. It is planned to test the model on completely artificial datasets to allow a more conclusive accuracy assessment. Another target is to provide a quantitative accuracy assessment of the radiometric calibration procedure for aerial images.

5 Acknowledgements

The author would like to thank Thomas Krauß (German Aerospace Center, Remote Sensing Technology Institute, Oberpfaffenhofen) for his useful advice. Special thanks go to Yunshan Li for her support throughout the generation of this work and help in formatting an earlier version of this paper.

6 Literature

- BARNESLEY, M., ALLISON, D. & LEWIS, P., 1997: On the Information Content of Multiple View Angle (MVA) images. *International Journal of Remote Sensing* **18**(9), 1937-1960.
- BARNESLEY, M. J., SETTLE, J. J., CUTTER, M. A., LOBB, D. R. & TESTON, F., 2004: The CHRIS/PROBA Mission: A Low-Cost Smallsat for Hyperspectral Multiangle Observations of the Earth Surface and Atmosphere. *IEEE Transactions of Geoscience and Remote Sensing* **42**(5), 1512-1520.
- CHEN, J. M., LI, X., NILSON, T. & STRAHLER, A., 2000: Recent Advances in Geometrical Optical Modelling and its Applications. *Remote Sensing Reviews* **18**(2-4), 227-262.
- D'ANGELO, P., 2007: Radiometric Alignment and Vignetting Calibration. *Proceedings of the 5th International Conference on Computer Vision Systems*, March 21-24, 2007, Bielefeld University, Germany.
- KIMES, D. S., 1983: Dynamics of Directional Reflectance Factor Distributions for Vegetation Canopies. *Applied Optics* **22**(9), 1364-1372.
- KOUKAL, T. & ATZBERGER, C., 2012: Potential of Multi-Angular Data Derived from a Digital Aerial Frame Camera for Forest Classification. *IEEE Journal of Selected Topics in Applied Earth Observations and Remote Sensing* **5**(1), 30-43.
- KOUKAL, T. & SCHNEIDER, W., 2010: Analysis of BRDF Characteristics of Forest Stands with a Digital Aerial Frame Camera. *The International Archives of Photogrammetry, Remote Sensing and Spatial Information Sciences* **38**(7A), 100-105.
- KURZ, F., TÜRMEER, S., MEYNBERG, O., ROSENBAUM, D., RUNGE, H., REINARTZ, P. & LEITLOFF, J., 2012: Low-Cost Optical Camera Systems for Real-Time Mapping Applications. *Photogrammetrie Fernerkundung Geoinformation* **2012**(2), 159-176.
- LEWIS, P., 1995: The Utility of Kernel-Driven BRDF Models in Global BRDF and Albedo Studies. *Proceedings of the International Geoscience and Remote Sensing Symposium* **95**, July 10-14, Firenze, Italy, 1995, 1186-1188.
- LUCHT, W. & ROUJEAN, J. L., 2000: Considerations in the Parametric Modelling of BRDF and Albedo from Multiangular Satellite Sensor Observations. *Remote Sensing Reviews* **18**(2-4), 343-379.
- NICODEMUS, F. E., RICHMOND, F. C., HSIA, J. J., GINSBERG, I. W. & LIMPERIS, T., 1977: Geometrical Considerations and Nomenclature for Reflectance. US Department of Commerce, National Bureau of Standards, Washington DC.
- RICHTER, R. & SCHLÄPFER, D., 2005: Atmospheric/Topographic Correction for Satellite Imagery. German Aerospace Center (DLR), Weßling, Germany.
- WANNER, W., LI, X. & STRAHLER, A., 1995: On the Derivation of Kernels for Kernel-Driven Models of Bidirectional Reflectance. *Journal of Geophysical Research: Atmospheres* **100** (D10), 21077-21089.
- WILLIAMS, L., 1978: Casting Curved Shadows on Curved Surfaces. *ACM Siggraph Computer Graphics* **12**(3), 270-274.